

A Comparison of Satellite and Ground-Based Retrievals of Cloud Properties Over the ARM SGP Site

Z. Li, F.-L. Chang, A. Trishchenko, and M. Cribb

Canada Centre for Remote Sensing

Ottawa, Ontario, Canada

Introduction

The impact of clouds on the Earth's radiation budget and so climate depends on their macrophysical and microphysical properties. Cloud optical depth, effective droplet radius, and emission temperature are three major parameters required for understanding their impact on climate (Fouquart et al. 1990, Slingo 1990). Numerous research efforts have devoted to retrieve these parameters from remote sensing. In general, the retrieval relies on the reflectance measured at a visible spectral channel to retrieve cloud optical depth; the reflectance measured at a near-infrared channel to retrieve cloud effective radius; and the emittance measured at an infrared channel to retrieve cloud emission temperature. For nearly two decades, the Advanced Very High Resolution Radiometer (AVHRR) onboard the National Ocean and Atmospheric Administration (NOAA) polar orbiting satellites have been used widely for the retrievals of cloud properties (Ran et al. 1994, Platnick and Twomey 1994, Nakajima and Nakajima 1995). AVHRR provided five spectral measurements at 0.63-, 0.89-, 3.7-, 11-, and 12- μm . However, comparisons with aircraft- and surface-based studies have reported that the droplet effective radii retrieved from remote sensing were systematically larger than those measured in situ (Nakajima and King 1991). Since the retrievals were based on the spectral reflectance measurements, they must be susceptible to the photon penetration depth that varies with the spectral channels and droplet size distributions. Miles et al. (2000) summarized that the vertical variability of droplet radius observed from in situ measurements proved to be large enough to affect the retrievals.

To better understand the role of clouds in the Earth's climate system, National Aeronautics and Space Administration (NASA) has recently commenced its largest earth observation mission, the Earth Observing System (EOS), which consists a series of space-based remote sensing platforms, e.g., the Tropical Rainfall Measuring Mission (TRMM), the morning platform Terra, and afternoon platform Aqua. Cloud observation onboard the TRMM is achieved by the Visible and Infrared Scanner (VIRS). VIRS offers potential improvements in calibration, spatial resolution, and retrieval of cloud particle size due to the inclusion of 1.6- μm channel, in addition to the popular 3.7- μm channel. In this paper, the satellite remote sensing schemes for retrieving cloud properties of optical depth, effective radius, and emission temperature are examined by using the VIRS satellite data. The retrieved cloud properties are compared with the ground measurements over the Atmospheric Radiation Measurement (ARM) southern great plain (SGP) central facility site. The cloud droplet effective radii retrieved using two different near-infrared channels, namely, 1.6- μm and 3.7- μm channels are also compared with those inferred from ARM at the ground level.

VIRS Data

The TRMM VIRS radiometer like the AVHRR consists of five spectral bands, but centered at about 0.64-, 1.6-, 3.7-, 11-, and 12- μm . The VIRS data has a pixel spatial resolution of approximately $(2 \text{ km})^2$ at nadir viewing angle. The equatorial orbiting TRMM satellite only made observations at low latitudes with the maximum viewing angle being limited to less than 50° . This study utilizes two different approaches for the retrievals of cloud properties. The first one uses a combination of 0.64-, 1.6-, and 11- μm channels and the second one uses a combination of 0.64-, 3.7-, and 11- μm channels. Figure 1 shows the normalized VIRS spectral response functions for the nominal 0.64-, 1.6-, 3.7-, and 11- μm channels. To account for atmospheric attenuation, each spectral channel was divided into six sub-wavelength intervals and its spectral response curve was averaged over the sub-wavelength intervals. For comparing with the ground-based retrievals from ARM, the VIRS data were obtained for a region covering a region of $\pm 1^\circ$ in latitude and longitude over the central facility of the ARM SGP site (97.5°W , 36.6°N). Such a region covers a geographical area of $\sim(90 \text{ km})^2$. The VIRS data analyzed here were collected on four overcast days over the ARM SGP site as listed in Table 1, along with solar and viewing zenith angles and relative azimuth angles. The threshold methods (Rossow and Schiffer 1991) were applied to both the VIRS 0.64- μm and 11- μm channels for the identification of cloudy pixels, which were then used for retrieving cloud optical depth (τ_c), droplet effective radius (r_e), and emission temperature (T_c) based on the two retrieval schemes.

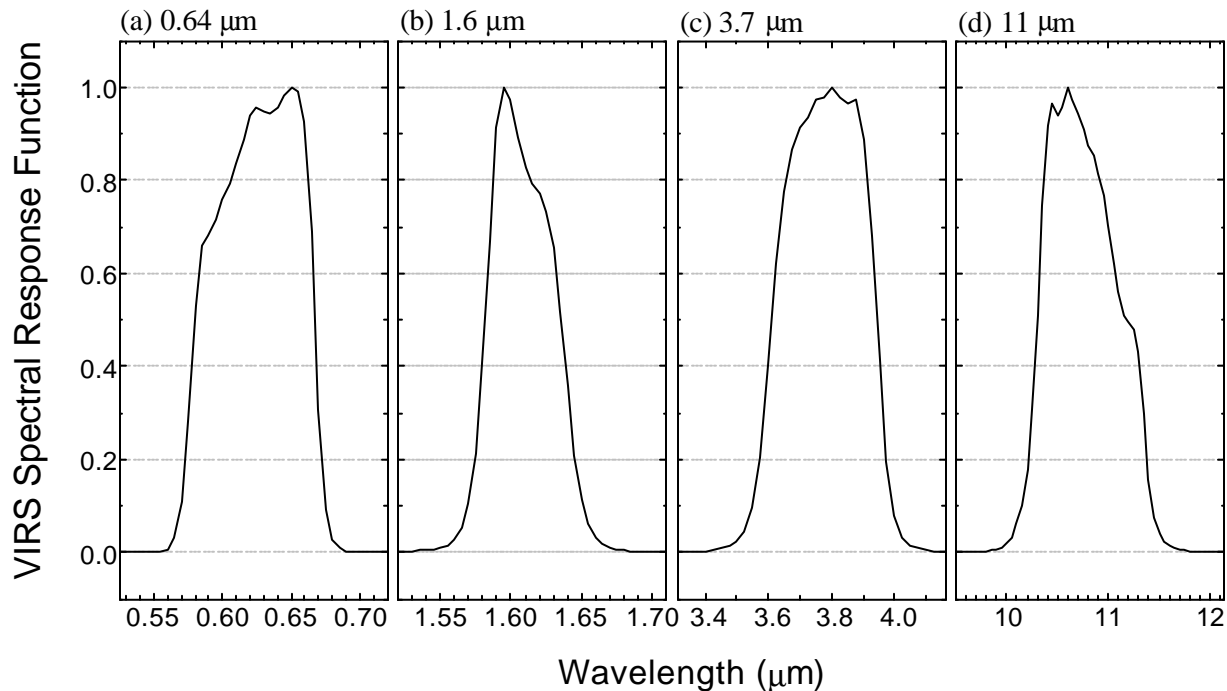


Figure 1. Normalized spectral response functions for VIRS 0.64-, 1.6-, 3.7-, and 11- μm channels.

Date	Solar Zenith Angle (deg)	Viewing Zenith Angle (deg)	Relative Azimuth Angle (deg)
1998/02/08	58.4-60.9	14.3-44.8	41.6-43.5
1998/03/30	38.3-40.7	14.4-44.4	34.2-37.1
1998/04/03	29.9-31.8	24.9-48.2	5.5-8.9
1998/08/11	44.9-47.1	11.4-42.9	77.8-80.5

Cloud Property Retrieval Scheme

The cloud property retrieval scheme adopts the lookup table method that was based on the radiative transfer modeling to compute reflected and emitted radiances for the channels selected. Cloud properties of τ_c , r_e , and T_c for individual cloudy pixel are retrieved by comparing VIRS radiance measurements to lookup-table radiances. Table 2 describes the procedures of the two retrieval schemes. The left column is for the 0.64-1.6-11- μm scheme and the right one is for the 0.64-3.7-11- μm scheme. It is noted that 1.6- μm measurements contain mainly reflected radiation, whereas 3.7- μm observations contain both reflected and emitted radiation that are significant and comparable in their magnitudes.

The lookup tables of the reflected and emitted radiances for VIRS 0.64-, 1.6-, 3.7-, and 11- μm channels were calculated for various cloud conditions using an adding-doubling radiative transfer model. The various cloud conditions were specified by three variables of τ_c , r_e , and cloud-top height (Z_c), including 12 different τ_c (0.1, 1, 2, ... 256), 13 different r_e (2, 3, 4, ... 30 μm), and six different Z_c (0, 1, 2, ... 9 km). The adding-doubling routine was performed at 16 Gauss quadrature points in both upward and

<u>0.64-1.6-11-μm scheme</u>	<u>0.64-3.7-11-μm scheme</u>
⇓	⇓
1. Initial guesses of $r_e = 10 \mu\text{m}$ and $Z_c = 1 \text{ km}$	
2. Retrieve τ_c by comparing VIRS 0.64- μm reflectance to lookup tables	
3. Retrieve T_c by comparing VIRS 11- μm emission to lookup tables	
4. Estimate Z_c by comparing T_c to vertical temperature profile from sounding data	
⇓	⇓
5. Retrieve r_e by comparing VIRS 1.6- μm reflectance to lookup tables	5. Calculate 3.7- μm emission contribution based on previous τ_c , r_e , T_c , and Z_c . Subtract the emission from VIRS 3.7- μm radiance to obtain the reflectance contribution. Retrieve r_e by comparing VIRS 3.7- μm reflectance to lookup tables.
⇓	⇓
6. Repeat steps 2 through 5 till all retrieved values converged to stable values	

downward zenith directions, so the lookup tables also spanned 16 solar zenith and satellite viewing zenith angles (5.90° , 13.52° , 21.12° , ... 89.97°) and 19 relative azimuth angles between the sun and satellite (0° , 10° , 20° , ... 180°). In the radiative transfer calculations, the Mie theory and lognormal size distribution were adopted for calculating cloud optical properties (Hansen and Travis 1974). The cloud layer was assumed to completely fill up a single layer with saturated humidity. The atmospheric column was divided into eight vertical layers (0–1, 1–2, 2–4, ... 25–100 km) with the gaseous concentrations adopted from LOWTRAN-7 model (Kneizys et al. 1988) to correct for the effects of molecular absorption and scattering. A Lambertian surface albedo of 0.1 was assumed for 0.64-, 1.6-, and 3.7- μm channels and the surface emissivities of 0.9 and 1.0 were assumed for 3.7- μm and 11- μm channels, respectively.

Retrieved τ_c , r_e and T_c

Figures 2 to 4 show the comparisons of the retrieved τ_c , r_e , and T_c that were derived using the two different retrieval schemes. The retrievals were performed for the cloudy pixels that were obtained from the VIRS satellite passes over the ARM SGP site on four different days. The total number of VIRS cloudy pixels was indicated in the figures. The comparisons showed generally good agreement in the retrieved τ_c and T_c . Some differences in the retrieved pixel T_c are due to the effect of thin clouds. As thin clouds are not opaque in the 11- μm channel, the retrieval of cloud emission temperature is thus very sensitive to small changes in cloud optical depth. The problem is often eased when cloud optical depth is larger than 5, where excellent agreement exists in terms of both the individual pixel and overall means.

On the other hand, the comparison of the two retrieved r_e exhibits tremendous discrepancies, the r_e inferred from 1.6- μm channel being generally larger than those inferred from 3.7- μm channel by about a factor of two. Such a large bias was attributed to the calibration error in the VIRS 1.6- μm radiances (Pat Minnis 2000, personal communications). In the 10th ARM Science Team Meeting (2000), Minnis presented a study of comparing the VIRS 0.64- μm and 1.6- μm reflectances with the coincident 0.64- μm and 1.6- μm reflectance measurements observed by the Along Track Scanning Radiometer (ATSR) that was on flight the European Space Agency's ERS-2 satellite. The simultaneous comparisons showed very good agreement (1:1) between the ATSR and VIRS 0.64- μm reflectance measurements, but large difference of approximately a factor of 1.2 was found in the ATSR 1.6- μm reflectance relative to the VIRS 1.6- μm reflectance. Due to such a discrepancy, the τ_c , r_e , and T_c was re-derived for the 0.64-1.6-11- μm retrieval scheme with an estimation of 20% increase in the 1.6- μm reflectance to account for the calibration error. Figure 5 shows the re-derived r_e (x-axis) and the r_e inferred from the 0.64-3.7-11- μm scheme (y-axis). The new comparisons show better agreement in the two retrievals. However, large difference still exists as the difference increases with increasing r_e . It is noted that the 20% increase applied here for correcting the 1.6- μm reflectance is only a rough estimate. More accurate calibration scheme for correcting the reflectance errors requires further data analysis, which should at least account for dependence on solar zenith angle and ground surface conditions, both having seasonal variations.

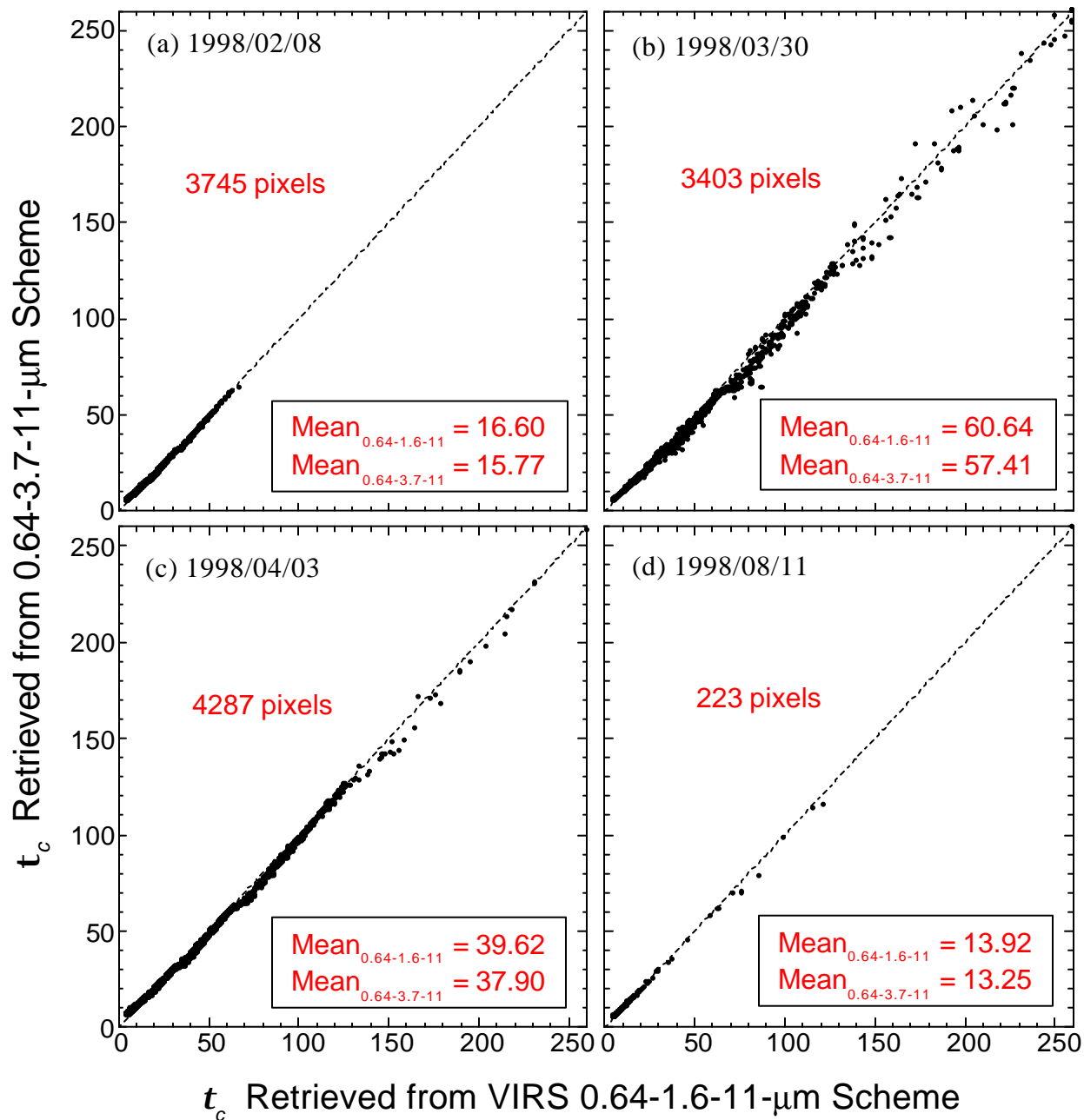


Figure 2. Comparisons of t_c retrieved from the VIRS 0.64-1.6-11- μm and 0.64-3.7-11- μm schemes. The dash line indicates the one-to-one relationship

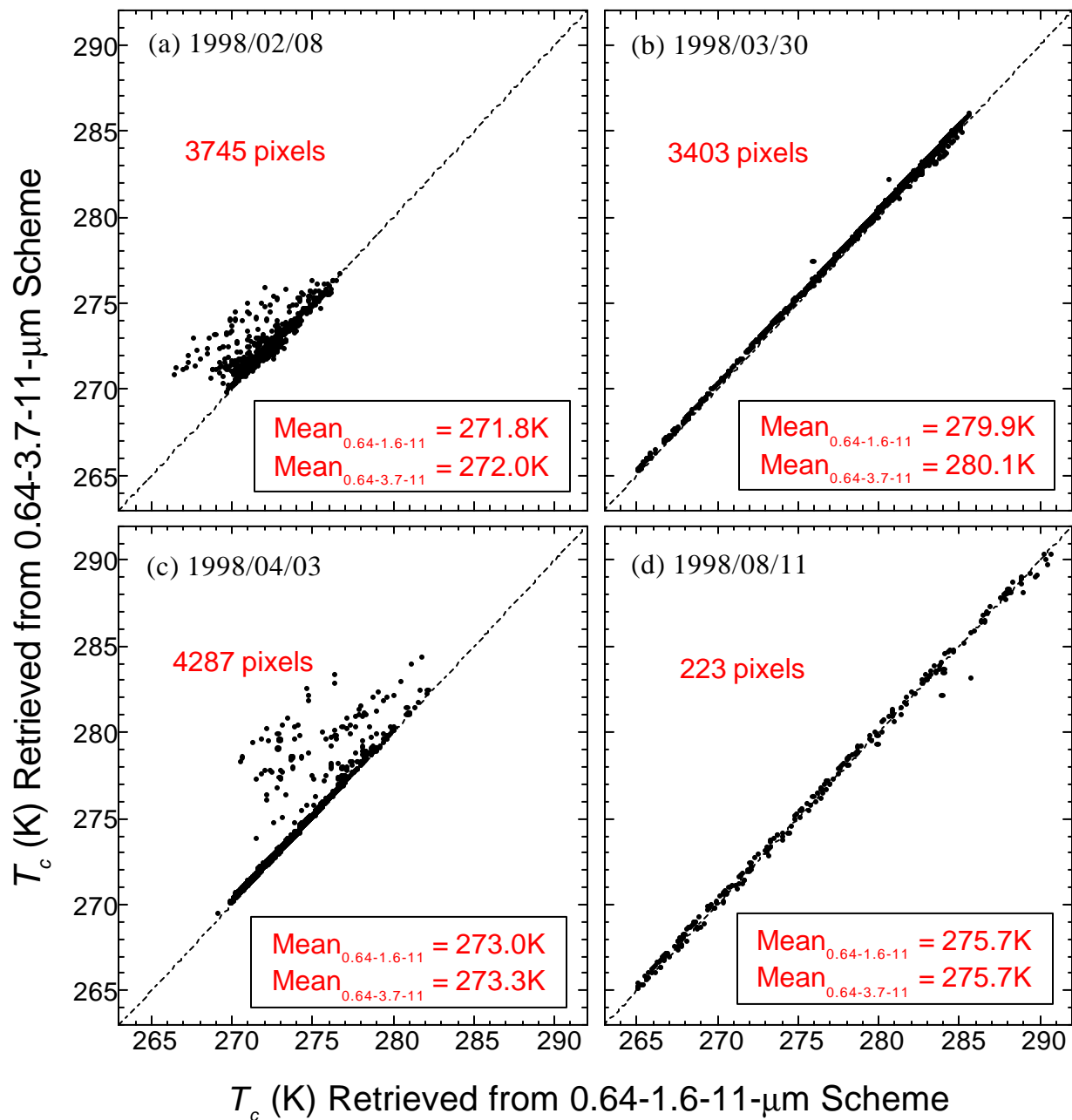


Figure 3. Comparisons of T_c (K) retrieved from the VIRS 0.64-1.6-11- μm and 0.64-3.7-11- μm schemes. The dash line indicates the one-to-one relationship.

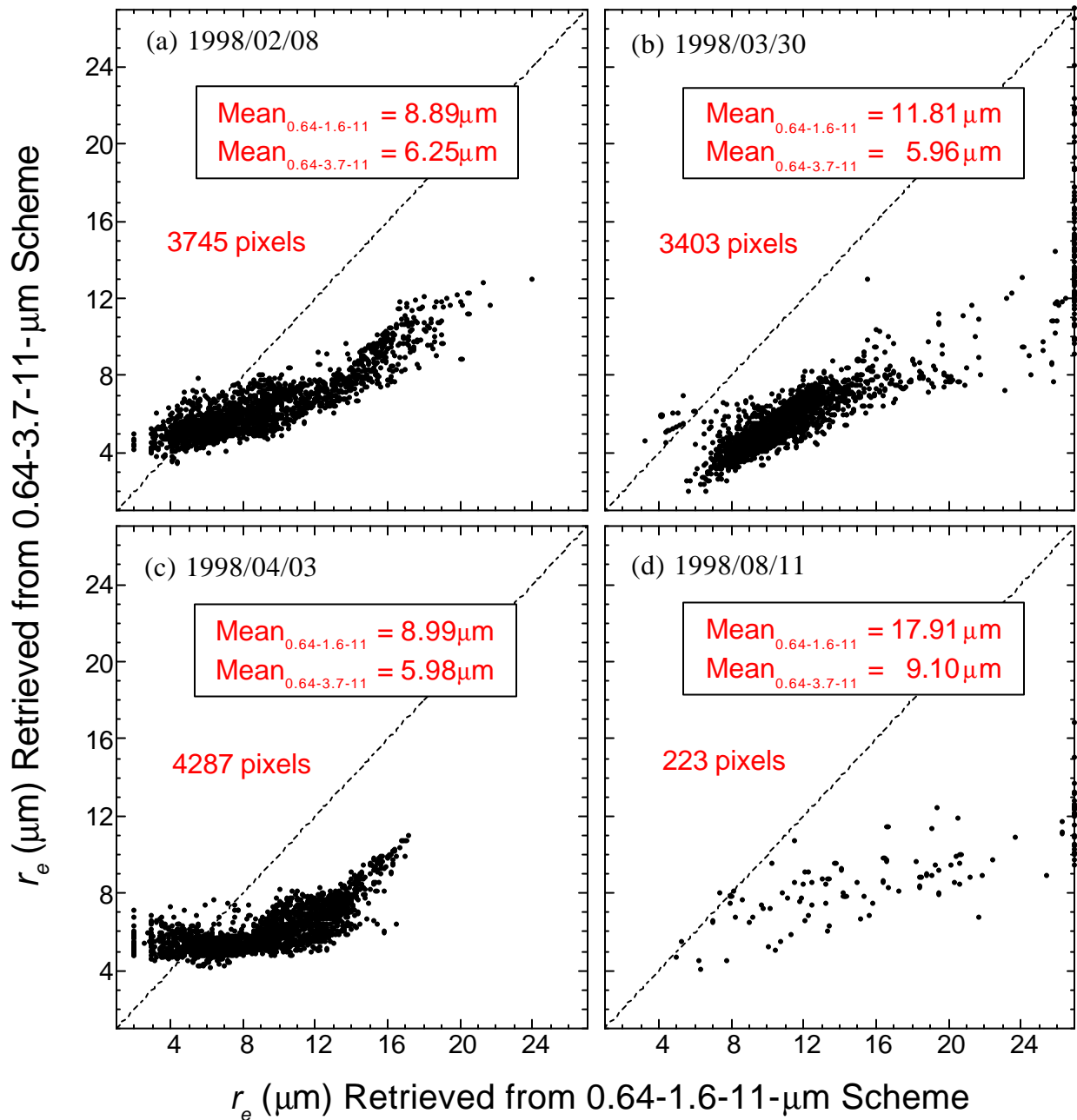


Figure 4. Comparisons of r_e (μm) retrieved from the VIRS 0.64-1.6-11- μm and 0.64-3.7-11- μm schemes. The dash line indicates the one-to-one relationship.

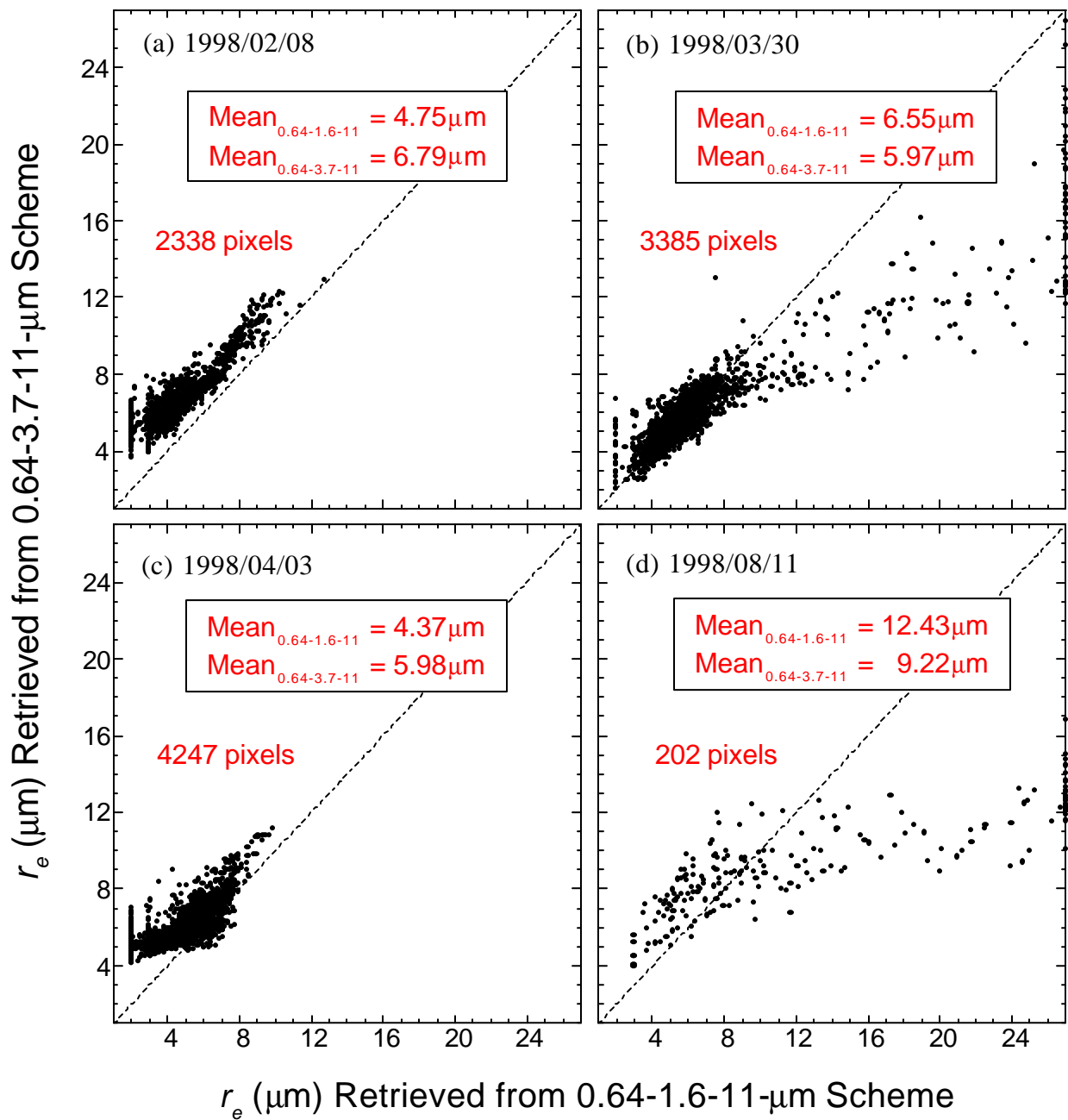


Figure 5. Comparisons of r_e (μm) retrieved from the corrected VIRS 0.64-1.6-11- μm and 0.64-3.7-11- μm schemes. The dash line indicates the one-to-one relationship.

The VIRS retrieved τ_c and r_e are further compared with the values inferred at ground level. Table 3 shows the comparisons obtained on four different dates. The ground-based inferred τ_c was retrieved using transmittance measurements observed by the Rotating Shadowband Spectroradiometer (RSS) deployed at the ARM SGP site. The retrieval was also based on the comparison with lookup tables that were generated by radiative transfer modeling. The r_e was then derived by $r_e = 1.5LWP/\tau_c$, where LWP denotes the cloud liquid water path retrieved from the microwave measurements obtained at the ARM SGP site. The comparisons between the VIRS satellite and ground-based retrievals showed large differences. Since the three retrievals are sensitive to different portions of a cloud, certain discrepancies are expected, compounded by some artificial effects such as sampling errors in space and time. The VIRS retrievals were averaged over a large spatial domain of $\sim 1^\circ \times 1^\circ$ (latitude \times longitude) for an instantaneous satellite overpass, whereas the ground retrievals were only obtained for a small upward-viewing area, but averaged over a period of a few minutes. Further studies are needed to better understand the differences.

Date	τ_c	r_e (mm)
	VIRS-0.64-1.6-11-mm / VIRS-0.64-3.7-11-mm / ground	VIRS-0.64-1.6-11-mm/ VIRS-0.64-3.7-11-mm/ground
1998/02/08	16.60 / 15.77 / 6.6	8.89 / 6.25 / 10.8
1998/03/30	60.64 / 57.41 / 49.9	11.81 / 5.96 / 6.0
1998/04/03	39.62 / 37.90 / 53.5	8.99 / 5.98 / 9.1
1998/08/11	13.92 / 13.25 / NIL	17.91 / 9.10 / NIL

Summary

This study attempts to use VIRS satellite data to retrieve cloud optical depth (τ_c), droplet effective radius (r_e), and emission temperature (T_c) on four overcast days over the ARM SGP site. In addition to having four channels similar to AVHRR, the VIRS satellite also carries a shortwave near-infrared channel at 1.6- μm , which provide independent information regarding the vertical variation in r_e . As conventional satellite cloud retrieval schemes have relied on AVHRR 0.64-, 3.7-, and 11- μm channels for the retrievals of τ_c , r_e , and T_c , this study compared the performance of two satellite retrieval schemes. The first scheme uses VIRS 0.64-, 1.6-, and 11- μm channels and the second uses VIRS 0.64-, 3.7-, and 11- μm channels. The two retrieval schemes showed similar retrieved τ_c and T_c , but very different r_e . The retrieved r_e from the 0.64-1.6-11- μm scheme were systematically larger than those from the 0.64-3.7-11- μm scheme, which was caused primarily by large calibration error in the VIRS 1.6- μm reflectance as noted by Minnis (2000, personal communications). A bias of 20% in the 1.6- μm reflectances between VIRS and ATSR results in considerable differences of a factor of 2 in the retrieved r_e values, which was confirmed by comparisons against ground-based retrievals using measurements from the Rotating Shadowband Spectroradiometer and microwave radiometer.

Acknowledgment

This work was supported by the US Department of Energy Grant DE-FG02-97ER62361 under the Atmospheric Radiation Measurement (ARM) program.

Reference

Fouquart, Y., J. C. Buriez, M. Herman, and R. S. Kandel, 1990: The influence of clouds on radiation: A climate-modeling perspective. *Rev. Geophys.*, **28**, 145-166.

Han, Q., W. B. Rossow, and A. A. Lacis, 1994: Near-global survey of effective droplet radii in liquid water clouds using ISCCP data. *J. Climate*, **7**, 465-497.

Hansen, J. E. and L. D. Travis, 1974: Light scattering in planetary atmospheres. *Space Sci. Rev.*, **16**, 527-610.

Kneizys, F. X., E. P. Shettle, L. W. Arbeau, J. H. Chetwynd, G. P. Anderson, W. O. Gallery, J. E. A. Selby, and S. A. Clough, 1988: Users Guide to LOWTRAN-7. Air Force Geophysics Laboratory Tech. Rep. AFGL-TR-88-0177, pp. 137.

Miles, N. L., J. Verlinde, and E. E. Clothiaux, 2000: Cloud droplet size distributions in low-level stratiform clouds. *J. Atmos. Sci.*, **57**, 295-311.

Nakajima, T. Y., and T. Nakajima, 1995: Wide-area determination of cloud microphysical properties from NOAA AVHRR measurements for FIRE and ASTEX regions. *J. Atmos. Sci.*, **52**, 4043-4059.

Nakajima, T. Y., M. D. King, J. D. Spinhirne, and L. F. Radke, 1991: Determination of the optical thickness and effective particle radius of clouds from reflected solar radiation measurements. Part II: Marine stratocumulus observations. *J. Atmos. Sci.*, **48**, 728-750.

Platnick, S., and S. Twomey, 1994: Determining the susceptibility of cloud albedo to changes in droplet concentration with the advanced very high-resolution radiometer. *J. Appl. Meteor.*, **33**, 334-347.

Rossow, W. B., and R. A. Schiffer, 1991: ISCCP cloud data products. *Bull. Amer. Meteor. Soc.*, **71**, 2-20.

Slingo, A., 1990: Sensitivity of the Earth's radiation budget to changes in low clouds. *Nature*, **343**, 49-51.